Hydrogeology Journal (2014) 22: 1807–1824
DOI 10.1007/s10040-014-1173-6

Use of artificial and natural tracers to assess groundwater transit-time distribution and flow systems in a high-alpine karst system (Wetterstein Mountains, Germany)

Ute Lauber · Nico Goldscheider

Abstract Groundwater in mountainous karst regions is vital for regional water budgets and freshwater supply. Owing to increasing water demand and climate change, detailed knowledge of the highly heterogeneous alpine aquifer systems is required. Multi-tracer analyses have been conducted in the steep karstic Wetterstein Mountains, which includes Germany's highest summit, Zugspitze (2,962 m asl). Results of artificial tracer tests demonstrate well-developed flow paths through the unsaturated zone (up to 1,000 m thickness). Flow paths cross topographic divides and contribute to deep drainage systems underneath alpine valleys. Cross-formational flow has been identified. Quantitative analysis of tailing-dominated breakthrough curves and stable isotopes (^{18}O) has enabled determination of the mean transit-time distribution. A fast-flow component with transit times between 3 and 13 days was found in karst conduits and open fissures, dependent on flow conditions. An intermediate-flow component, showing mean transit times of about 2.9–4.9 months, was found in well-drained fissures and fractures. A slow-flow component with mean transit times greater than 1 year is attributable to slow flow and low storage in the poorly drained fissures and rock matrix. The conceptual model enables a better understanding of drainage, water resources and vulnerability of the high-alpine karst system.

Keywords Karst · Alpine hydrogeology · Tracer tests · Stable isotopes · Germany

Received: 28 November 2013 / Accepted: 21 July 2014
Published online: 23 August 2014

U. Lauber (✉) · N. Goldscheider (✉)
Institute for Applied Geosciences, Division of Hydrogeology, Karlsruhe Institute of Technology (KIT), Kaiserstr. 12, 76131, Karlsruhe, Germany
e-mail: ute.lauber@kit.edu
Tel.: 0721-608 45061
e-mail: goldscheider@kit.edu

Introduction

Alpine regions are characterized by high precipitation leading to substantial surface runoff and/or groundwater recharge. Alpine areas form headwaters for regional river systems such as the Danube and the Rhine, and other large regions benefit from the abundance of water (Viviroli and Weingartner 2004). In the Alps, there are some well-known examples where alpine water resources are used to supply major cities with drinking water, e.g. Vienna and Innsbruck in Austria, and Grenoble in France; however, in most alpine aquifer systems, recharge processes, drainage systems and potentially available water resources are still insufficiently known (Goldscheider 2011). Amongst others, the main challenges are strong heterogeneity and variability: recharge processes highly depend on temporal and spatial distribution of snowmelt and precipitation, drainage follows heterogeneous geologic structures and groundwater volumes are difficult to quantify as groundwater levels and hydraulic rock properties (e.g. porosity, aperture width of fissures, fracture network and karstification) are often not known. In addition, conventional hydrogeological investigation techniques are often difficult to use in alpine regions.

Nevertheless, climate change and population growth has contributed to an increasing awareness of alpine hydrogeology in the past decade. Future changes in local precipitation, snow cover patterns and glacier storage are likely to affect runoff in alpine headwaters (Bates et al. 2008). Population growth results in increasing demand for drinking-water supply, irrigation of agricultural areas and industrial water. As alpine (karst) water resources are likely to become even more important in the future, an increasing number of studies focus on this topic. Interdisciplinary approaches include meteorological research combined with snow and catchment hydrology to characterize the dynamic water resources in mountainous karst regions (Kraller et al. 2012; Marke et al. 2013). Hydrogeological mapping and hydrogeochemical techniques are applied to evaluate the water quality of the available resources (Simsek et al. 2008). Other studies use assessment methods to characterize karst morphology and groundwater vulnerability, considering epikarst, vegetation, infiltration and the karstic network to have a major influence on transit time (Perrin et al. 2004; Plan et al. 2009). Spring hydrograph analysis and hydrochemical methods allow for characterization of infiltration processes of the saturated and

unsaturated zone (Mudarra and Andreo 2011) and enable determination of drainage structures, transit times and recharge processes of alpine karst aquifers (Wetzel 2004; Ozyurt and Bayari 2008; Mudarra et al. 2014). Mean transit times and transit-time distribution have been demonstrated to be an important aspect for understanding dynamic groundwater storage, variable water quality and vulnerability to contamination (Bakalowicz 2005; Worthington 2007; Müller et al. 2013).

Tracer methods are particularly suitable to assess transit times and flow properties in alpine aquifers, partly because the necessary equipment is manageable. In recent studies, artificial tracer tests were applied in high-alpine karst systems to resolve the influence of heterogeneous geologic structures on karst drainage and recharge processes (Goldscheider 2005; Gremaud et al. 2009; Goldscheider and Neukum 2010; Finger et al. 2012; Kübeck et al. 2013; Mudarra et al. 2014). Tracer tests, conducted under variable flow conditions, have revealed variability of transit times by a factor of 5 or more (Göppert and Goldscheider 2008; Gremaud et al. 2009). As artificial tracers are generally injected into preferential flow paths, flow properties of the conduit system are investigated that result in short transit times and high flow velocities; however, these tracers omit the fissured-porous matrix of the aquifer, which plays an important role with respect to water storage and karst water volumes (Maloszewski et al. 2002; Worthington 2007). To investigate the matrix of karst systems, the use of stable isotopes as natural tracers has been established over the past few decades (Dewalle et al. 1997). Analyses of stable isotopes in spring water allow for estimating transit times of the water, identifying sources and mixing of water as well as calculating water volumes in the alpine aquifer (Rodgers et al. 2005; Einsiedl 2005). In contrast to artificial tracer tests, where only preferential flow paths are considered, stable isotope analyses offer the possibility to observe long-term properties of aquifer systems. For these reasons, the combination of artificial and natural tracer tests is particularly favorable to elucidate transit-time distribution in the aquifer.

Facing climate change and increasing water demand, the objective of this study is to develop a conceptual model of a high-alpine karst aquifer in Germany, in the Wetterstein Mountains. The area is part of the headwater of the Loisach River, providing runoff for the city of Munich and the surrounding countryside. Special characteristics of this area are steep topographic gradients, a karst aquifer of up to 1,000 m thickness and an unsaturated zone that is almost as thick as the whole aquifer. By combining artificial and natural tracer techniques, this study offers insights into transit-time distribution and flow systems in the karst conduit network and in the fissured-porous rock matrix of the alpine karst aquifer. The research allows a first assessment of drainage systems and karst water volume, which is needed to manage and to protect the water resources for further generations.

Field site

Geological setting and karst development

The Wetterstein Mountains are located in the German Alps close to Garmisch-Partenkirchen—700 m above sea level (asl). They consist of three mountain ridges, including Germany's highest summit, the Zugspitze (2,962 m asl); Fig. 1. The remote, high alpine valleys between the three ridges, Reintal and Höllental are accessible only by foot (Fig. 2). The difference in elevation between valley floors and summits is up to 2,200 m. Above 2,000 m asl, most areas are poorly covered by alpine and nival vegetation (Fig. 1) (Küfmann 2003). Two cirques around the highest summit (Höllental and Zugspitz cirques) are still partially covered by vestigial glaciers. With a total extent of about 55 ha and a mean thickness of 12 and 17 m, respectively, the two glaciers (Höllentalferner and

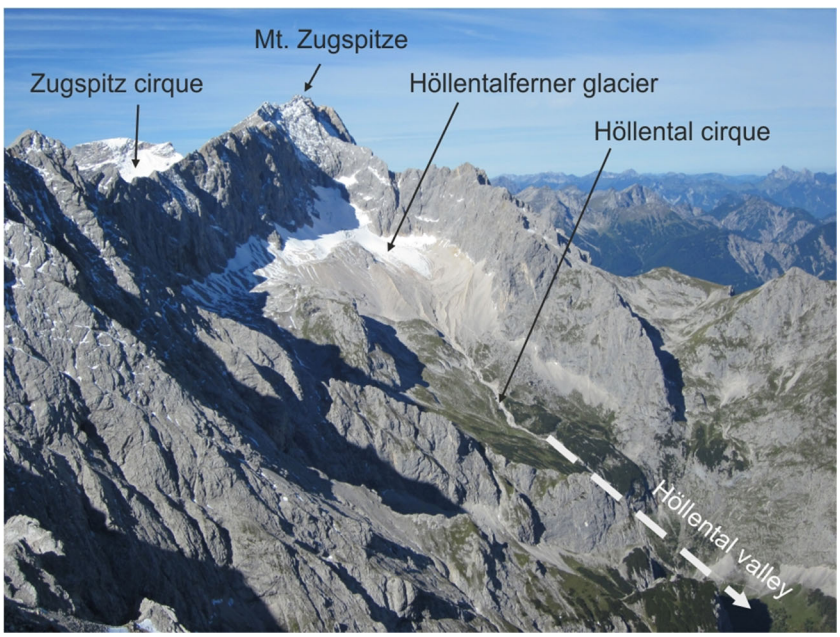

Fig. 1 Impression of the steep Wetterstein Mountains with the highest summit, *Zugspitze* (2,962 m asl), and the remaining glacier (*Höllentalferner*). The massive mountain ridges are formed by the up-to-1,000-m-thick Wetterstein limestone, the main karst aquifer

 DOI 10.1007/s10040-014-1173-6

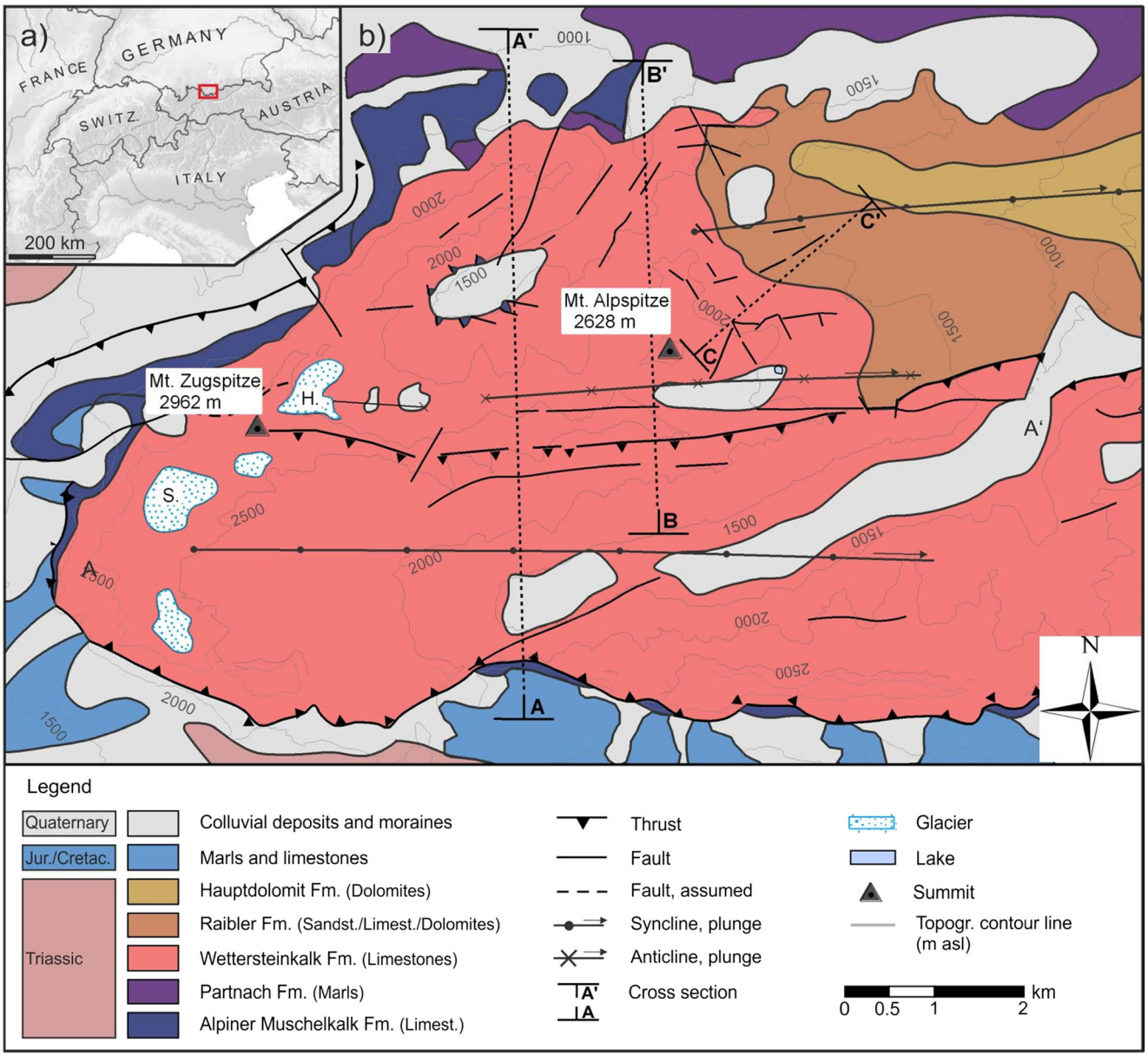

Fig. 2 **a** Map of the study site (Wetterstein Mountains) in the German Alps and **b** Geologic and tectonic setting of the Wetterstein Mountains. The Wettersteinkalk Fm. constitutes the main karst aquifer; glaciers: Höllentalferner (*H*) and Schneeferner (*S*). Geological cross sections are shown in Figs. 3, 8 and 9

Nördlicher Schneeferner) are the largest remaining glaciers in Germany (Hagg et al. 2012).

The Wetterstein Mountains formation includes the up-to-1,000-m thick Triassic Wetterstein limestone (Fig. 2), which can be divided into three groups: a lower, thick and massive reef limestone, a well-bedded limestone, and an upper limestone. There are no distinctive marker horizons within the entire limestone formation, which complicates the determination of stratigraphic positions (Fig. 3). Particularly in the northern parts of the area, the marly Partnach Fm. occurs at the base of the karst aquifer, partially substituting the limestone. The underlying strata consist of a sequence of marls and well-bedded limestones (Alpiner Muschelkalk Fm.) that act as an aquitard, depending on the fraction of marls. The strata are folded and form two regional synclines and one regional anticline, which appear as valleys and ridges (Fig. 3). The fold axes trend W–E and plunge to the east (20–35°). The entire Triassic stratigraphy belongs to the Lechtal nappe of the East Alpine (Austro Alpine) nappe system and has been thrusted over Jurassic and Cretaceous series to the southeast and south (backthrust; Vidal 1953; Bögel 1960; Miller 1961).

Since the Eocene, the region has generally been steadily uplifting; high mountain chains have dominated the landscape since the early Oligocene (Frisch et al. 2008). Karstification is particularly evident at the cirques, where the slopes are less steep and precipitation and meltwater seep directly into the karst aquifer. At Zugspitz cirque for example, various small- to

DOI 10.1007/s10040-014-1173-6

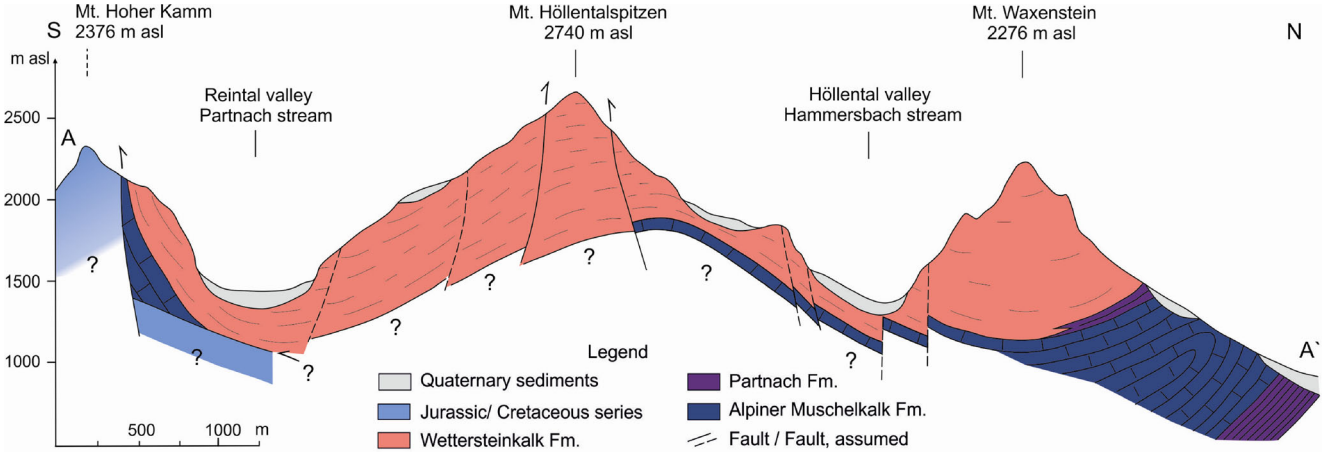

Fig. 3 Geological cross section *A–A′* of the Wetterstein Mountains; the three mountain ridges and the two valleys are formed by thick limestone, the main karst aquifer. The cross section is not vertically exaggerated

medium-sized caves are known; surface karst structures like dolines and karren occur frequently. Strong weathering and karstification together with intensive soil development occurred after the glacial retreat about 11,500 years ago (Grüger and Jerz 2010); however, no larger cave systems are known in this area. In contrast to the cirques, only a few karst features exist in areas where the slopes are steep and vegetation is low. In these areas, physical weathering results in strong jointing so that predominant gravitational erosion aggravates the evolution of prominent karst structures. To date, uplift is highest in this part of the Alps with rates of about 1 mm/year (Frisch et al. 2008).

Hydrogeology

Several karst springs emanate into alpine streams and rivers flowing east to northwards into the foreland (Fig. 4). The Hammersbach Stream has cut deep into the limestone and forms an approximately 100 m deep and narrow gorge in the northern Höllental Valley. There are four main karst springs

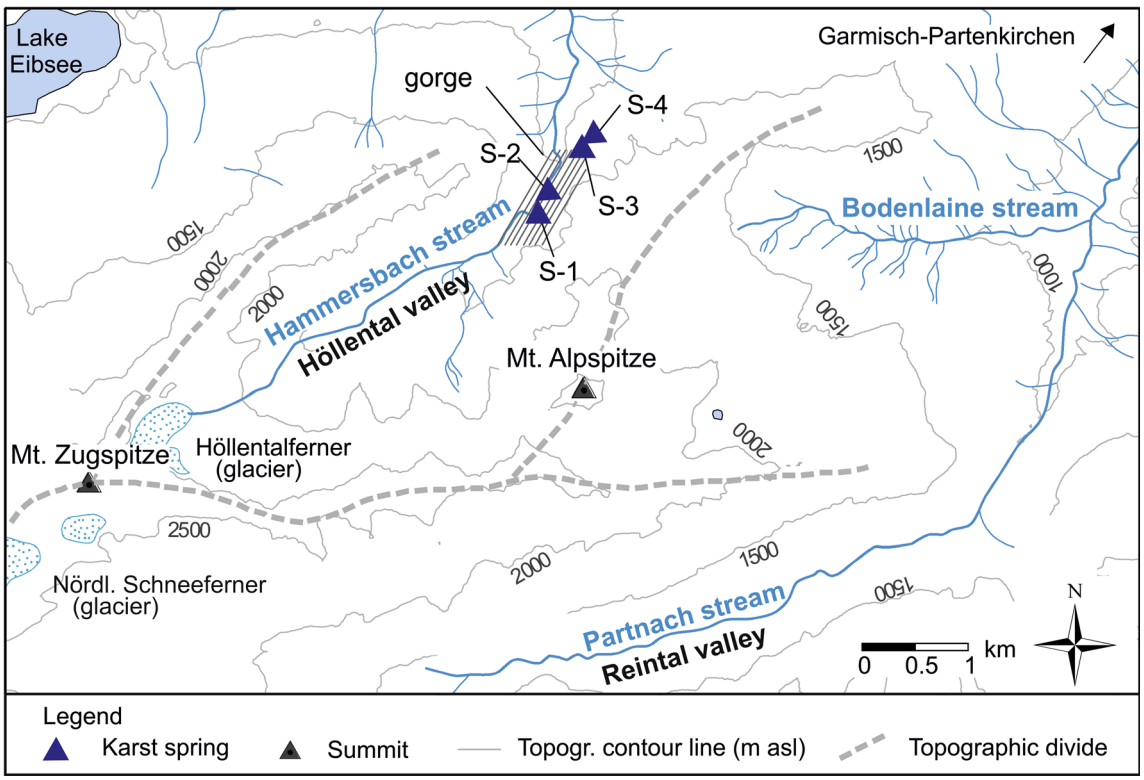

Fig. 4 Mountain ridges, glaciers, surface waters in the main valleys and selected karst springs in the Wetterstein Mountains; *dashed lines* indicate topographic water divides

 DOI 10.1007/s10040-014-1173-6

in the northern valley (Fig. 4, Table 1): Spring S-1, a spectacular karst spring, is situated at a fault zone at the eastern rock face of the gorge. Having a mean runoff of about 260 L/s, water discharges from a karst conduit and falls down into the Hammersbach Stream (Fig. 5); thus, only indirect measurements of tracer concentrations are possible by sampling upstream and downstream of the tributary. S-2 is a small spring located at a fault zone on the western side in the gorge at the level of the hiking trail. The discharge of the karst conduit is about 7 L/s and the two springs, S-1 and S-2, are perennial. Springs S-3 and S-4 are waterfalls on steep rock faces located at the eastern rock face of the gorge. The exact elevations of the spring orifices are not known. S-3 is an intermittent spring with a mean discharge of about 12 L/s during summer months and without discharge in late autumn. S-4 is also intermittent with a high discharge of up to 200 L/s in wet periods of early summer. The spring responds rapidly to rain and snowmelt events, while in dry periods, the spring runs dry after several days of no rain.

The water temperature of spring S-2 is representative of the mean annual temperature of groundwater in the catchment area. Hydrochemical properties of the three springs S-2 to S-4 are similar. Ca^{2+}, Mg^{2+} and HCO_3^- are the major ions, as is typical for groundwater from limestone. The electrical conductivity of the three karst springs is between 150 and 165 μS/cm, reflecting low mineralization. The content of total dissolved solids is between 110 and 170 mg/L.

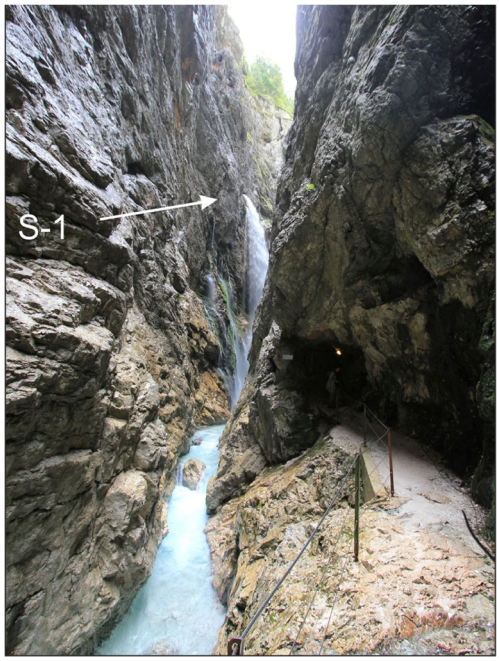

Fig. 5 View in southern direction from the hiking trail into the gorge to spring *S-1*; direct sampling at S-1 is not possible

Material and methods

Artificial and natural tracers

Two artificial tracer tests have been conducted in the area around Mt. Alpspitze to resolve transit time distributions and drainage structures in the karst conduit system. The fluorescent dye uranine (CAS 518–47–8) was used as the solute tracer.

In 1998, an injection of uranine (2 kg) was performed on the 25th of September. The injection point was located in a small cirque at an elevation of 2,200 m asl and was selected to define catchment areas and water divides between three alpine valleys, the northern, northeastern and southern valley (Fig. 6). The tracer was added to runoff of a small intermittent karst spring, which was seeping into the karst aquifer a few meters below the spring, with a discharge of about 0.2 L/s. The injection was conducted after several days without rain. Data have been used to delineate spring catchments but have not been analyzed quantitatively (Goldscheider et al. 1999).

Table 1 Main karst springs in the lower Höllental Valley (northern valley of the study area) and their physiochemical characteristics

Spring No. Name		S-1 Klamm spring	S-2 Tunnel spring	S-3 Gorge entrance spring	S-4 Rotgraben spring
Description		Waterfall at E side of the gorge	Spring at W side of the gorge	Waterfall at E side of the gorge	Waterfall at E side of the gorge
Elevation	[m asl]	~ 1,180	~ 1,100	~ 1,100	~ 1,100
Discharge (min/max)	[L/s]	260 (105/490)	7 (4/9)	12 (0/24)	- (0/200)
Type	[−]	Perennial	Perennial	Intermittent	Intermittent
Temp.	[°C]	NA	4.5	NA	NA
EC	[μS/cm]	NA	148	157	163
pH	[−]	NA	8.3	8.3	8.2
Ca^{2+}	[mg/L]	NA	22.0	23.5	24.1
Mg^{2+}	[mg/L]	NA	4.5	3.8	3.9
Na^+	[mg/L]	NA	0.3	0.2	0.1
K^+	[mg/L]	NA	0.1	0.1	0.1
Cl^-	[mg/L]	NA	0.4	0.3	0.2
NO_3^{2-}	[mg/L]	NA	1.2	1.7	1.5
SO_4^{2-}	[mg/L]	NA	0.7	0.8	1.1
HCO_3^-	[mg/L]	NA	98	104	104

NA not analyzed; no direct measurement at the source is possible

 DOI 10.1007/s10040-014-1173-6

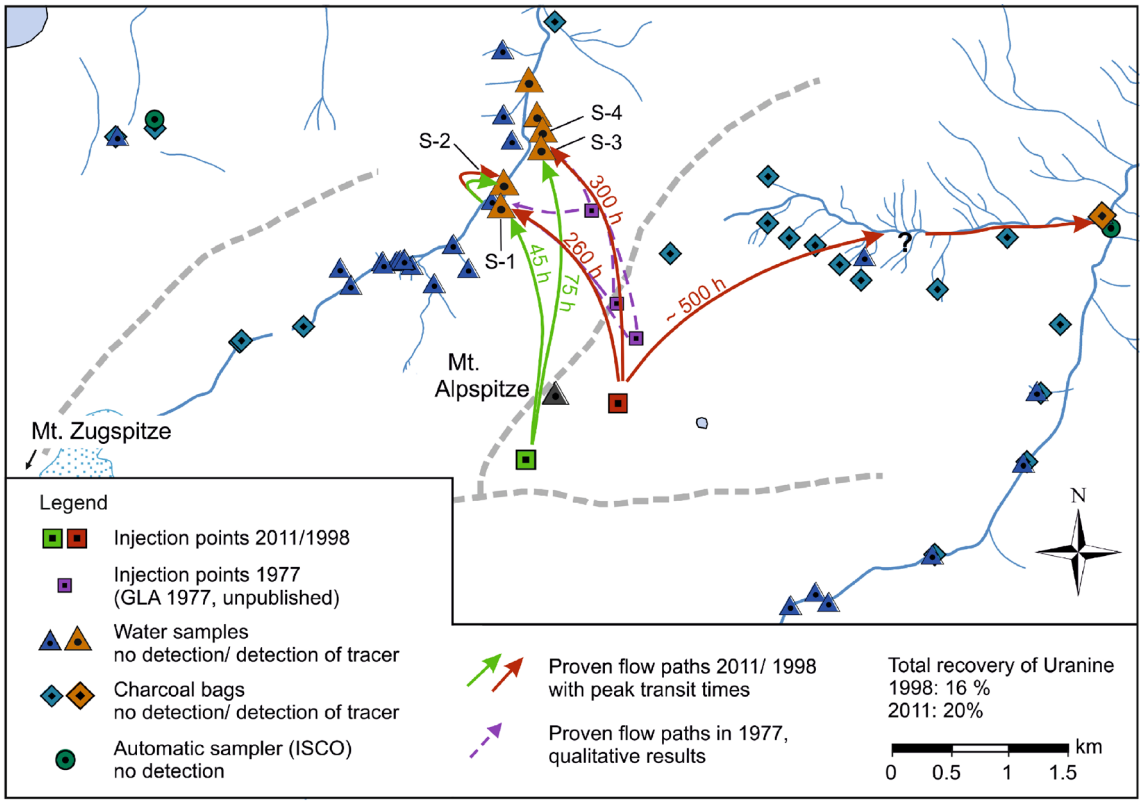

Fig. 6 Injection points and sampling locations during the two tracer tests, with the location of the four selected karst springs *S-1* to *S-4*. *Dashed lines* indicate topographic divides. Transit time is in hours

In 2011, 4 kg of uranine were injected on the 16th of July at a central cirque in the Wetterstein Mountains at a location, where meltwater of a remaining snowfield was seeping naturally into the aquifer (Figs. 6 and 7). The injection point was located beyond the apparent topographic catchment area of the northern valley at an elevation of 2,350 m asl. High precipitation before and after the injection-facilitated drainage through the unsaturated zone. Surrounding valleys were observed by water samples and charcoal bags, whereas at selected sites, automatic samplers (ISCO) were installed.

Two Perkin Elmer spectro-fluorometers (LS 50 B and LS 55) were used to measure uranine in water samples and charcoal bags. The synchronous-scan method was utilized. For calculation of tracer recoveries, discharge measurements were conducted by using the salt-dilution method.

There are data available on previous tracer tests conducted by the Geological Survey in 1977—Bayerisches Geologisches Landesamt (GLA), unpublished report, 1977 (Fig. 6). In that study, the tracers uranine, eosine and sulphorhodamine G were used as tracers

Fig. 7 Injection of uranine in July 2011 in the central area of the Wetterstein Mountains at an elevation of about 2,350 m asl

 DOI 10.1007/s10040-014-1173-6

and injected on August 1977 north of Mt. Alpspitze. Qualitative results of the three injections are taken into account in this study in order to resolve drainage structures.

For further characterization of transit-time distribution in fissured-porous rock matrix, isotopic data were collected from the springs. Stable isotopes of oxygen and deuterium were used as natural tracers; samples were collected between May 2011 and October 2012. Sampling intervals were mainly dependent on weather conditions; no sampling was feasible in winter (November to May) due to inaccessibility of the area (deep snow cover and risk of avalanches). During summer, samples were collected once per month in 2011 and every 2 weeks in 2012.

Climate and isotope data

Climate data were acquired from nearby weather stations, managed by Deutscher Wetterdienst (DWD). One weather station is situated in the community of Garmisch-Partenkirchen, located at 719 m asl, while a second weather station is located on the summit of the Zugspitze, 2,959 m asl (Fig. 2).

The mean monthly air temperature in Garmisch displays a minimum of −2 °C in December and January, and a maximum of 17 °C in July and August. At the Zugspitze, temperatures are approximately 10 °C colder than at Garmisch. The total annual precipitation in 1998 was 1,440 mm in Garmisch and 2,180 mm at the Zugspitze, whereas in 2011, the total annual precipitation was lower with 1,215 mm in Garmisch and 1,780 mm at the Zugspitze; precipitation is well distributed over both years (1998 and 2011).

Isotopic data for precipitation at surrounding observation stations were acquired from the Global Network of Isotopes in Precipitation (GNIP) and the Austrian Network for Isotopes in Precipitation (ANIP). Together with isotopic data from Zugspitze, which was provided by the Institute of Groundwater Ecology of the Helmholtz Research Institute in Munich, data were used to estimate the altitude effects in the area. Long-term isotopic data from Garmisch for the years 1978–2009 were used to evaluate seasonal variability of isotopes in precipitation and to estimate mean transit time of water.

Data analysis and modeling

The main direction of flow and hydraulic connections between injection points and springs were determined by positive tracer detection. Basic parameters of the flow system were directly obtained from observed breakthrough curves (BTCs): Maximal flow velocities (v_{max}) were determined with respect to time of first detection (t_0); based on main breakthrough and peak concentration (c_P), dominating transit times (t_{dom}) and velocities (v_{dom}) were derived. To allow comparison, BTCs were normalized by dividing observed concentrations by the injected tracer mass; the resulting unit is m^{-3}.

Using a simple advection-dispersion model (ADM) implemented in the program CXTFIT (Toride et al. 1999), first estimates for mean flow velocities (v) and longitudinal dispersion (D_L) were obtained. Due to the skewness of the BTCs, fitting of the curves lead to coefficients of determination (R^2) of only 0.8. A better fit for the right-skewed BTCs was desired, so, BTCs were modeled with the two-region nonequilibrium (2RNE) model of CXTFIT, which has been successfully applied to characterize transport in karst aquifers (Field and Pinsky 2000; Geyer et al. 2007; Göppert and Goldscheider 2008; Mudarra et al. 2014). By accounting for mobile and immobile fluid phases, the model leads to good fits of the asymmetric BTCs ($R^2>0.9$) but less robust values by reason of altogether four fitting parameters; however, the shape of highly irregular BTCs can also result from a combination of two or more peaks provoked by dominating flow components in the turbulent core of karst conduits and laminar flow along margins of the conduit (Massei et al. 2006; Mudarra et al. 2014), variable flow rates or multiple flow paths (Field and Leij 2012). In the present case, the skewness of the BTCs also indicates the presence of two peaks, whereas the second and lower ones are completely hidden in the long tail. For quantitative evaluation, a multi-dispersion model (MDM) was applied, delineated by Käss (2004) and implemented in the program TRACI95.

For interpolating seasonal trends of variation and to obtain mean annual values, the isotopic signal in precipitation and spring water were fitted by a seasonal sine wave curve (Dewalle et al. 1997; Rodgers et al. 2005):

$$\delta^{18}O = y_0 + A[\cos(ct-\theta)] \quad (1)$$

where $\delta^{18}O$ is the modeled isotopic signal, y_0 is the mean annual $\delta^{18}O$, A is the annual amplitude of the signal, c is the radial frequency of annual fluctuations (0.017214 rad/day), t is the time in days after beginning of sampling, and θ is the phase lag or time of the annual peak $\delta^{18}O$ in radians. Amplitudes and uncertainties of the parameters were obtained by fitting the function. Available data for isotopes in precipitation were used in this study. To obtain the input-signal, the weighted monthly mean values from Garmisch (years 1978–2009) were corrected by the mean elevation of the catchment area. As this approach does not account for spatial distribution of precipitation within the catchment area and does not include the years 2011 and 2012 (for which data were not available), isotopic values were, therefore, interpreted for 2011 and 2012 by correlating monthly air temperatures and isotopic values for other available years. In snow-dominated alpine catchments, snow accumulation during winter and isotopic contribution of snowmelt in spring and early summer will cause a delay of the input of isotopic depleted winter recharge. Because of the large differences in elevation, temporal and spatial variability of snow accumulation and snowmelt can be expected and evaporation from snow and fractionation processes during

 DOI 10.1007/s10040-014-1173-6

snowmelt affect the isotopic compositions of snowmelt input. Because of the high number of unknowns and scarce data in the area, the long-term monthly mean values provide an estimate of the input-signal. Müller et al. (2013) calculated the effects of different input-signals on transit time estimates in an alpine catchment in the Swiss Alps. According to their findings at transit times of 65–105 weeks, there was variation of 10–23 % between different input-signals.

To estimate mean transit time of the natural tracer, isotopic data were modeled using the lumped-parameter approach implemented in the software FLOWPC (Maloszewski and Zuber 1982). The simple structure of the model requires only a few input parameters and, therefore, is suitable to apply in alpine catchment areas, where data are often scarce (Maloszewski et al. 1992, 2002; Müller et al. 2013). By calculating predefined impulse-response functions [g (τ)] and transit times (τ), the isotopic input signal $\delta^{18}O_{IN}$ is fit to observed values at the spring $\delta^{18}O_{OUT}$.

$$\delta^{18}\mathrm{O18}(t) = \int_0^\infty \delta^{18}\mathrm{O}_{\mathrm{IN}}(t-\tau)g(\tau)d\tau \qquad (2)$$

The best fit is obtained by trial and error and is quantitatively described by the goodness of the fit, i.e. the root mean square error (RMSE) and the efficiency of the model (EM; Maloszewski and Zuber 2002). In this study area, the data could be well fitted with the impulse-response function [g (τ)] of an exponential model and a dispersion model. The exponential model, however, was preferred based on the assumption that groundwater flow through the thick unsaturated zone occurs along individual fissures and karst structures in the catchment area. Infiltrating water follows individual flow lines and mixing processes only occur shortly before the outlet. This approach has been applied in alpine catchment areas with thick unsaturated zones (Maloszewski et al. 1992; Müller et al. 2013). The dispersion model can also account for mixing processes in the unsaturated zone of alpine aquifers (Maloszewski et al. 1992, 2002). The long tailing of the observed BTCs (artificial tracers) indicate that there is at least some water exchange between conduits and fissures; however, the use of the dispersion model requires estimation of two additional parameters, the dimensionless dispersion parameter P_D ($= D_L/vx$) and the fitting coefficient β, which indicates the proportion of an "old" groundwater component (Maloszewski and Zuber 2002). While these parameters can be estimated (e.g. Maloszewski et al., 2002), the resulting additional uncertainty yields less robust results. The exponential model provides a simpler and less ambiguous approach, and is applied herein. Given the relatively simple structure of the lumped-parameter model and the low number of input data points, results are estimates, but are nonetheless useful.

In addition to the fresh infiltrated water moving through larger fissures, there is generally a slow flow component of the groundwater, which is older than the fresh infiltrated water and contributes to the baseflow of the spring. The isotopic composition at the spring shows a mixture of "old" groundwater and fresh infiltrated water. Using the exponential model, the proportion of the slow flow component was estimated by analyzing the transit-time distribution.

With additional information from discharge measurements, recovery was determined. Conduit volumes (V) were estimated by multiplying the mean discharge (Q_{mean}) and the mean transit time of tracer (t_{mean}) (Field and Nash 1997).

Results and discussion

General results of the tracer test in 1998

Uranine was detected at several springs in the northern and in the northeastern valley (Fig. 6). Breakthrough curves of S-1, S-2 and S-3 show one clear peak and a long tailing. The first detection of uranine was at S-1 and S-2 193 h after injection; maximum concentrations of 1.3 μg/L were reached after 260 and 335 h respectively. At S-3, a maximum of 1.6 μg/L was measured after 260 h. Peak flow velocities vary between 6 and 9 m/h. Discharge of the springs were largely constant except at S-4, where large variations in spring discharge from 0 to 100 L/s were observed, together with a multi-peaked BTC; the peaks can be related to the discharge, however, with results discussed in the following.

Recoveries at single springs were quite low and ranged between 0.3 and 8.1 %, with total recovery in the northern valley about 16 %. This finding can be related to tracer injection very close to the anticline structure in the central area of the Wetterstein Mountains and is apparently a result of deep infiltration of the tracer and a contribution to regional flow systems (Fig. 8).

Results indicate that topographic divides do not correspond with underground catchment areas. Underground flow paths cross the mountain ridge of Mt. Alpspitze and contribute to the drainage of the northern valley (Fig. 6). Furthermore, there are obviously flow paths underneath the northern valley itself: uranine was also detected at S-2, at the opposite side of the valley. Between the injection point and S-2 lies the gorge, which cuts deep into the limestone. This is clear evidence for deep flow paths crossing beneath the gorge and demonstrates the presence of deep karst structures (Fig. 8). In addition, uranine was also detected in the northeastern valley, where most springs are related to the upper stratigraphic unit, the Raibler Fm. (Figs. 2 and 6); however, tracer was not detected at the individual springs but rather in the Bodenlaine Stream in the valley floor. As uranine must flow from the karst aquifer through the upper strata to emerge to the stream, the positive detection is evidence for cross-formational flow. Drainage follows either direct flow paths or deep flow systems to the valley (Fig. 9). In contrast, results of the tracer test in 1977 (GLA, unpublished report, 1977) showed only drainage to the northern valley; no tracer was detected in the

 DOI 10.1007/s10040-014-1173-6

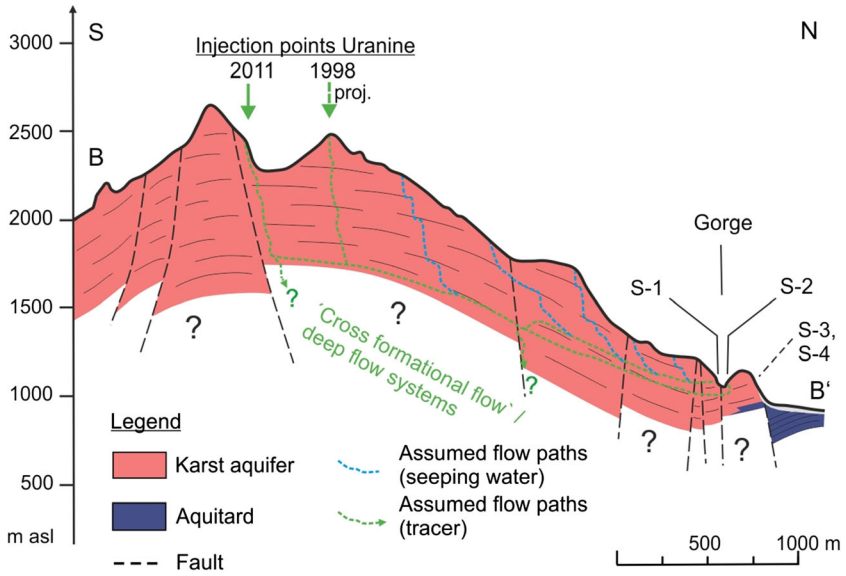

Fig. 8 Geological cross section *B–B′* between injection points and springs *S-1* to *S-4*. There is a deep but rapid flow system crossing below the deep gorge. The cross section is not vertically exaggerated

Bodenlaine Stream, which demonstrates the strong heterogeneity of the karst drainage, as discussed further in the following.

The results of 1998 were modeled with the MDM; calculated parameters are listed in Table 1. The multi-peaked BTC of S-4 was not modeled, as the multi-peaks are not a result of several flow paths but are connected to variable runoff at the spring; therefore, only the first peak was modeled.

General results of the tracer test in 2011

In 2011, underground drainage to the northern valley was observed, although the injection site is located south of the topographic divide. This finding is in accordance with results from 1998; however, no evidence for flow systems to the south or to the valley in the northeast has been found (Fig. 6). All breakthrough curves show one single peak and a long tailing. After 44 h, the tracer reached springs S-1 and S-3, while at the same time, the maximum of

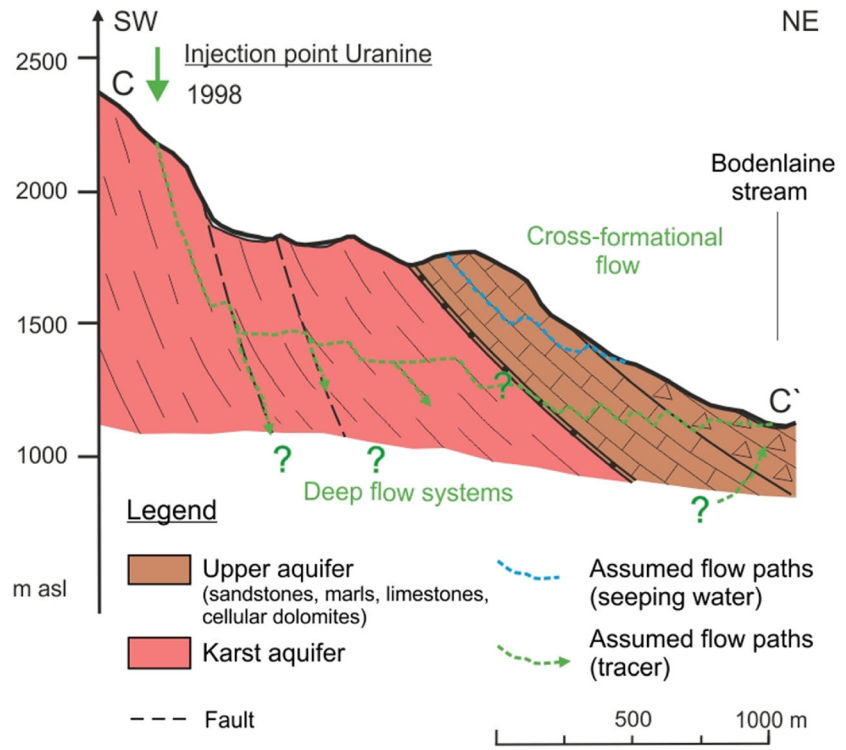

Fig. 9 Geological cross section *C–C′* between the 1998 injection point and the valley in the NE. There is cross-formational flow from the karst aquifer through the overlaying formations towards the discharge zone. The cross section is not vertically exaggerated

 DOI 10.1007/s10040-014-1173-6

21 μg/L was reached at S-2, confirming the existence of a deep but rapid flow system crossing below the deep gorge (Fig. 8). After 77 h, maximum concentrations between 5 and 10 μg/L were detected at the other springs, which results in peak flow velocities of 36–63 m/h.

Uranine was still detected at S-2, S-3 and S-4 for a sampling campaign in 2012, more than 1 year later. Concentrations were up to 0.2 μg/L, which is 100 times below maximum concentrations in 2011 but still 100 times above the detection limit (Fig. 10). It was not possible to detect low tracer concentrations at S-1, as direct sampling of the spring was not possible. The concentrations at springs S-2 to S-4 fluctuate and give evidence for dilution effects after rain events (Fig. 10). Tracer concentrations declined over the summer down to the detection limit in October 2012, suggesting remobilization of tracer stored in the karst system in 2011. Similar observations were made by Rappl et al. (2010) in the adjacent catchment area of Partnach spring.

Recovery was between 0.9 and 13 % at individual karst springs; total recovery of uranine in the northern valley was 20 % in 2011. Due to the sampling in 2012, recovery increased at S-2 from 0.8 to 1.3 %; at S-3, the increase was from 1.0 to 2.9 % and at S-4 it was from 3.7 to 4.0 %; thus, a noteworthy proportion of tracer had been stored in the karst system and released during the following year.

The results in 2011 confirm that there are flow paths crossing the topographic divide to S-1 and the deep gorge to S-2 (Fig. 8). At S-2, highest concentrations and flow velocities were observed proving well-developed drainage structures and deep karst flow paths are present; however, uranine concentrations at the nearby S-1, located on the SE side of the gorge and thus closer to the injection point, were significantly lower (5 μg/L) than at S-2 (21 μg/L). In contrast to S-2, the water-rich S-1 receives inflow from local water sources causing a higher dilution of the tracer (Fig. 8). Differences of flow times and velocities are likely to be a result of hydraulic gradient, as S-2 is located about 80 m lower than S-1. The results of the analytical modeling (MDM) are listed in Table 2, discussed in the following and selected BTCs are graphically shown in Fig. 11.

Hydrologic variability of the karst drainage network

BTCs show one main peak with a steep rising limb and a long tail, which can be separated into two individual BTCs by analytical modeling with a multi-dispersion model (Fig. 11). Thus, the main peak can be related to a BTC representing high mean flow velocities between 35 and 42 m/h in 2011 (Fig. 11; Table 2). These high flow velocities are attributable to advective and turbulent flow in karst conduits and open fissures. Considering the great thickness of the unsaturated zone, transit times of 50–80 h are short. There must be well-developed flow paths within the highly fractured and moderately karstified limestone. The skewness of the BTCs indicates strong tailing effects along the flow path. Analyses with the multi-dispersion model (MDM) for 2011 data revealed that the observed tailing effects are related to a second smaller peak caused

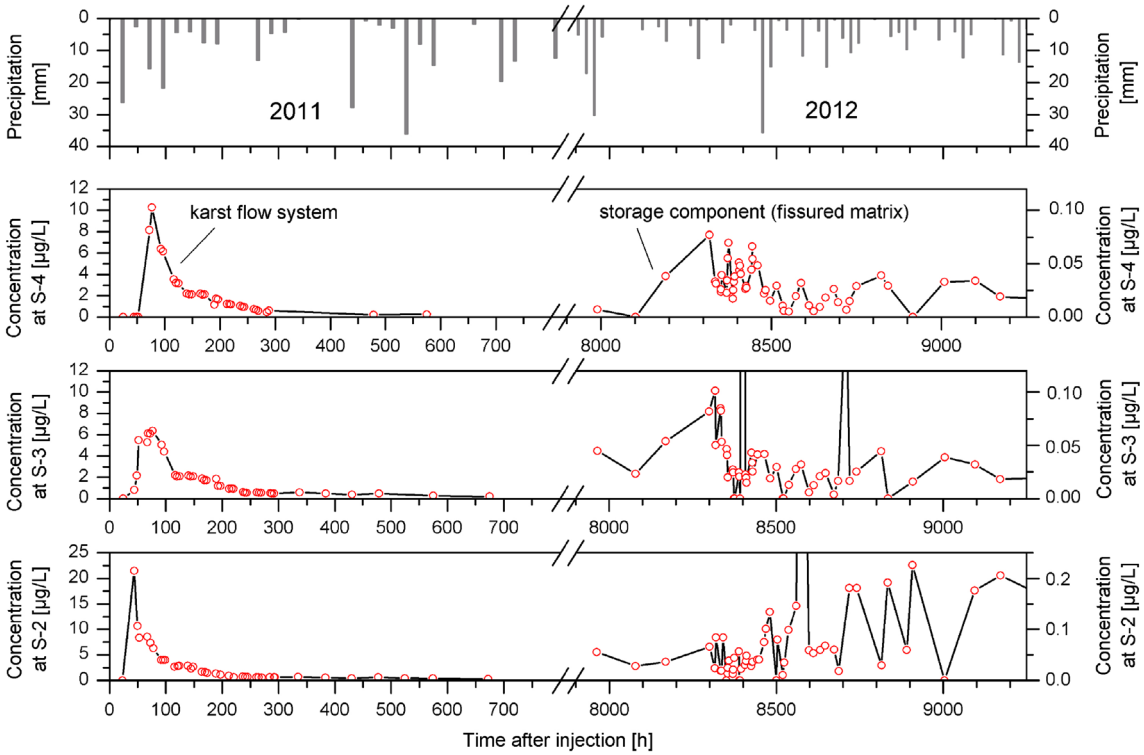

Fig. 10 Uranine breakthrough curves at three karst springs *S-2*, *S-3* and *S-4*; for a more detailed graphic presentation of the low uranine concentrations in 2012, the *right y-axis* scaling is by the factor of 100 lower than the *left y-axis* scaling. Precipitation data were obtained at the weather station Garmisch (DWD)

 DOI 10.1007/s10040-014-1173-6

Table 2 Aquifer parameters for karst conduits obtained from artificial tracer tests (uranine)

Spring No.			S-1		S-2		S-3		S-4		Overall comparison		
Test year			1998	2011	1998	2011	1998	2011	1998	2011		1998	2011
General parameters													
Injected tracer mass	M	[kg]	2.0	4.0	2.0	4.0	2.0	4.0	2.0	4.0	Ave.	2.0	4.0
Distance to spring	x	[m]	1,980	2,200	1,980	2,200	2,350	2,800	2,350	2,800	Ave.	2,202	2,560
Time of first detection	t_1	[h]	193.4	43.8	193.5	44.0	208.3	44.3	282.8	72.5	Ave.	219	49.72
Maximal flow velocity	v_{max}	[m/h]	10.2	50.2	10.2	50.0	11.3	63.3	8.3	53.7	Ave.	10.20	56.16
Peak transit time	t_p	[h]	260.1	43.8	335.0	44.0	258.8	76.8	306.8	77.0	Ave.	293	63.72
Peak flow velocity	v_p	[m/h]	7.6	50.1	5.9	50.0	9.1	63.3	7.7	36.4	Ave.	7.6	41.86
Peak concentration	c_p	[µg/L]	1.3	5.1	1.0	21.5	1.6	6.4	1.0	10.3	Max.	1.6	21.5
Normal peak concentration	c_p/M	[m^{-3}]	6.50E-07	1.28E-06	5.00E-07	5.38E-06	8.00E-07	1.60E-06	5.00E-07	2.58E-06	Max.	8.0E-07	5.4E-06
Conduit volume	V	[m^3]	–	73,907	–	1,308	–	4,032	–	19,902	Sum	–	99,149
Recovery	R	[%]	8.17	13.01	0.34	0.76	0.80	2.57	0.27	3.80	Sum	16.3	20.2
Modeled parameters (MDM)													
1st peak													
Mean flow velocity	v_{mean}	[m/h]	7.7	40.4	–	42.3	8.1	35.2	7.5	34.4	Ave.	7.8	38.1
Mean transit time (calc.)	t_{mean}	[h]	258	54	–	52	288	80	313	81	Ave.	286	67
Longitudinal Dispersion	D_L	[m^2/h]	133	5,770	–	5,883	204	3,087	40	1,305	Ave.	126	4,011
Dispersivity	α	[m]	17	143	–	139	25	88	5	38	Ave.	16	102
Peclet number	Pe	[–]	116	17	–	15	94	31	438	73	Ave.	216	34
2nd peak													
Mean flow velocity	v_{mean}	[m/h]	4.0	12.7	–	15.3	4.1	16.2	–	16.7	Ave.	4.1	15.2
Mean transit time (calc.)	t_{mean}	[h]	495	172.4	–	143	572	172	–	166.7	Ave.	534	164
Longitudinal Dispersion	D_L	[m^2/h]	505	4,890	–	3,583	570	2,107	–	2,754	Ave.	538	3,334
Dispersivity	α	[m]	126	385	–	234	139	130	–	165	Ave.	133	229
Peclet number	Pe	[–]	15	8	–	9	16	21	–	17	Ave.	16	14
Coeff. of determination	R^2	[–]	0.946	0.929	–	0.927	0.951	0.987	0.962	0.991	–	–	–

DOI 10.1007/s10040-014-1173-6

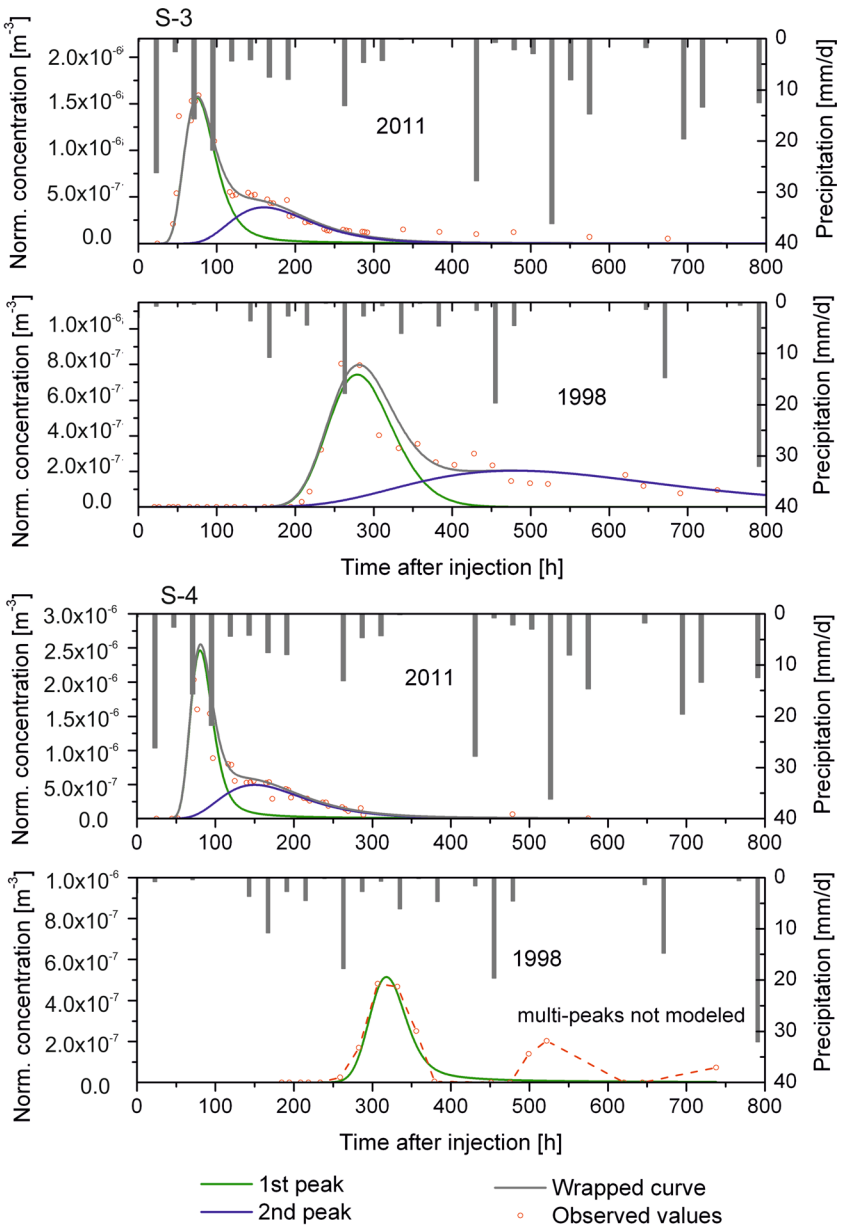

Fig. 11 Comparison of uranine breakthrough curves at *S-3* and *S-4*, observed and modeled values (multi-dispersion model MDM) from the tracer tests in 1998 and 2011, and precipitation (obtained by DWD, Garmisch)

by dominating flow velocities between 11 and 18 m/h. These intermediate flow velocities are 2–3 times smaller than the observed high flow velocities. Such flow velocities are generally found along rough margins of a main flow channel (Massei et al. 2006), smaller fissures, strata boundaries and stagnant zones; furthermore, the observed tailing is related to exchange with immobile fluid regions along the flow path, which occur in the thick unsaturated zone and result in persistent tracer concentrations 1 year after the injection.

Meltwater and precipitation before and after the injection of the tracer facilitated flow through the unsaturated zone. The injection points of the two tracer tests were located around Mt. Alpspitze in the central areas of the mountains. Distances to springs were in 2011 only slightly longer than in 1998. In 2011, the mean flow velocities were about 38 m/h on average and thereby 4–5 times higher than in 1998 (7.8 m/h; Fig. 11; Table 2). Whereas the average of mean transit times was about 286 h in 1998, mean transit times in 2011 were only 66 h and thus 4–5 times shorter. The observed variability of transit times can be related to weather conditions and seasonal differences between the two tracer tests. In 1998, the tracer test was conducted at the end of September. The month was generally rainy with light snowfall above 2,000 m, but there were several days without rain shortly before and after the injection. In 2011, however, the tracer test was conducted in the middle of July in a period with high precipitation. The days before the injection had been rainy; up to 28 mm of rainfall per day was measured

 DOI 10.1007/s10040-014-1173-6

during the first week of the tracer test. In addition, there is generally a significant component of snowmelt recharging the karst aquifer during early summer. According to Wetzel (2004) and Rappl et al. (2010), the contribution of snowmelt to the annual runoff is about 30 %; the peak is reached in July. As a consequence, the preferential flow paths through the unsaturated zone were fully wetted, and smaller fissures were completely filled with water, especially in July 2011.

The great hydrologic variability of the underground drainage of the karst system is coupled with variable tracer concentrations. In 2011, normalized tracer concentrations were significantly higher than in 1998 (Fig. 11; Table 2). Values vary by a factor of 2–5. Several studies have described the relations between flow conditions and maximum tracer concentrations in karst aquifers (Göppert and Goldscheider 2008; Pronk et al. 2007, 2009). In this case, higher flow velocities result in narrower BTCs and, therefore, higher maximum concentrations.

In 1998, tracer breakthrough at S-4 showed variability of tracer concentrations resulting in a multi-peak BTC (Fig. 11). The peaks are directly linked with spring discharge: uranine concentrations increase with increasing discharge, whereas a decrease of concentration was observed with decreasing discharge of the spring (Goldscheider et al. 1999), which suggests that the catchment area enlarges during high-flow conditions as a result of overflow. Tracer from the adjacent injection point can reach the spring and concentrations rise. With the decline of the water level, hydraulic connections are inactive and the catchment area is reduced to a local area. Then, only water from a local origin reaches the spring, resulting in a decrease of uranine concentrations. In contrast, a continuous BTC was observed in 2011, when the spring did not cease flow during the main sampling period. All observed aspects affirm high-flow conditions in 2011: high precipitation and snowmelt led to rapid tracer transport and high spring discharge. Steady high-flow conditions in July 2011 resulted in a continuous BTC; the catchment area of S-4 did not vary during the main breakthrough of the tracer.

Results with stable isotopes as natural tracers

The long-term weighted monthly means at Garmisch show a clear seasonal signal of isotopes in precipitation with a minimum of −14.6 ‰ $\delta^{18}O$ in December and a maximum of −7.0 ‰ $\delta^{18}O$ in July. The annual mean is −11.2±2.8 ‰ and the amplitude of the signal is 3.9±0.17 ‰. In the area, the altitude effect results in a depletion of −0.16 ‰ per 100 m (Fig. 12; Table 3), which is in good agreement with values from the Swiss Alps determined by Schürch et al. (2003) and Müller et al. (2013). The $\delta^{18}O$ values in precipitation were corrected by the mean topographic elevation of the catchment area of 2,000 m, resulting in a shift of the input-signal to annual mean values of −13.2± 2.8 ‰.

The seasonal variations are distinct in the isotopic signal at the springs. S-4 had the highest variation during the sampling period, at −13.7 ‰ $\delta^{18}O$ in May and −10.0 ‰ $\delta^{18}O$ in August. S-2 and S-3 show slightly lower variation (Fig. 12). The observed data were modeled and interpolated using Eq. (1) only for the summer months, due to inaccessibility of sampling sites in the mountains in winter. The annual means of isotope values at the springs and the uncertainties are between −13.9±0.7 ‰ and −13.2±0.4 ‰ $\delta^{18}O$, indicating that the recharge areas are at elevations between 1,800±250 and 2,300±430 m asl (Fig. 12). Considering the uncertainties, including a lack of winter values and the curve fitting, the springs are assumed to have the same catchment area, which is consistent with tracer tests indicating that the catchment area of the three springs is located around Mt. Alpspitze; the mean elevation is 2,000 m asl (Fig. 6). The amplitude of the input signal, 3.8±0.17 ‰, decreases down to values between 1.8±0.25 ‰ and 2.8±0.81 ‰ $\delta^{18}O$ at the three springs; there is also a distinct phase lag between input and output signal, varying between 1.1 and 1.8 months (Table 3). Considering the statistical monthly variability of 2 ‰ for isotopes in precipitation and the statistical uncertainties of the amplitude of the springs, which can exceed 0.8 ‰ because of the lack of winter samples, the amplitudes of the spring data are statistically within the same range. The spring discharge originates from the same groundwater flow component of the aquifer. The fact that the seasonal amplitude of the output signal is still distinctive at all three springs clearly indicates that the mean transit time is less than 1 year (Trček and Zojer 2009).

To quantify the transit times <1 year, observed $\delta^{18}O$ values at the springs were fitted with the exponential model. Isotopic input values, interpolated by the monthly mean temperature did not result in a good fit of the model, as the years 2011 and 2012 were about 1 °C warmer and the isotopic annual mean of the 2 years is, therefore, about 1 ‰ heavier compared to the annual mean of the springs. Best fitting of the data was obtained by using the long-term weighted annual mean values resulting in mean transit times between 2.9 and 4.9 months (Table 3). Although there are uncertainties regarding the input- and the output-signal, the obtained transit times are in good accordance with observed spring characteristics. The mean transit time is highest, at a value of 4.9 months, for S-2, which had a constant discharge over the observation period and to the authors' knowledge does not cease flowing. Shorter transit times of approximately 2.9–3.3 months were estimated for S-3 and S-4, both of which have a greater variability of discharge and are perennial, with flow ceasing after dry periods in late summer and autumn. Because of the intermittent discharge, fewer water samples were collected from S-4, resulting in the most uncertain results and lowest efficiency of the model (Table 3). The proportion of water that is younger than the mean transit time was derived by the distribution of the transit times and is between 53 and 57 % for the different springs, which indicates that about

DOI 10.1007/s10040-014-1173-6

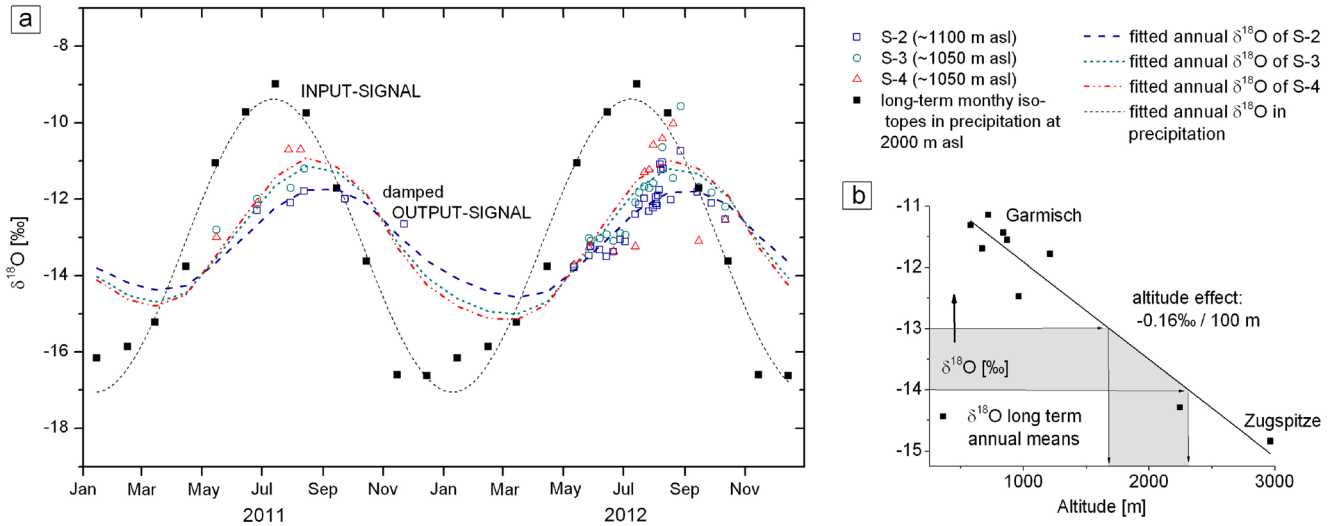

Fig. 12 **a** Seasonal $\delta^{18}O$ variations in precipitation (weighted monthly mean values at Garmisch, corrected by elevation), and at the springs *S-2*, *S-3* and *S-4*; monthly values of precipitation are fitted by a sine wave curve (Eq. 1) and by the exponential model of FLOWPC. **b** Shows the altitude effect in the area

43–47 % of the discharge is older than the mean transit times and roughly about 22–27 % is older than twice the mean transit time. In conclusion, there is a proportion of water that is at least older than 6–10 months. Considering results of Maloszewski et al. (1983, 1992, 2002), it is likely that the long-term flow component has a mean transit time of several years.

Conceptual model of underground drainage and karst aquifer parameters

Most of the observed karst springs in the northern valley are situated at fault zones, indicating that karst development and drainage is strongly linked to tectonic weak zones; thus, drainage structures are highly heterogeneously distributed in the massive limestone. In the area around Mt. Alpspitze, drainage of the karst aquifer is not controlled by topographic divides. Results of tracer tests with injections in 1977, 1998 and 2011 demonstrate a preferential drainage towards the steep and deep gorge in the north. In this case, drainage structures cross topographic divides, i.e., mountain ridges (Fig. 6). Uranine was found in spring S-2, located at the opposite side of the 100-m-deep gorge. Velocities of flow to that spring and associated tracer concentrations were the highest of all observed results in 2011. Consequently, there are well-developed and deep drainage structures crossing beneath the narrow gorge with the Hammersbach Stream (Fig. 8). Additionally, drainage to the gorge occurs transversely to the dip of the fold axis. In comparison with the other two alpine valleys in the Wetterstein Mountains, the Hammersbach Stream has cut the deepest into the karst aquifer. The gorge lies at a relatively low elevation between 1,000 and 1,100 m asl; as a result of the high hydraulic gradients, drainage is mainly toward this valley.

Table 3 Mean transit times of natural tracer obtained from stable isotope analysis. *SD* standard deviation

Component	Unit	Input-signal[a]	Spring S-2	Spring S-3	Spring S-4
Observed data					
Number of samples	[–]	24	42	34	28
Mean $\delta^{18}O$[b]	[‰]	−13.2	−13.4	−13.2	−13.9
SD[b]	[‰]	0.1	0.2	0.4	0.7
Amplitude[b]	[‰]	3.8	1.8	1.9	2.8
SD[b]	[‰]	0.2	0.3	0.4	0.8
Phase lag[b]	[months]	–	1.8	1.6	1.1
Exponential model					
Mean transit time (MTT) of tracer	[months]	–	4.9	3.3	2.9
Proportion of water older than 1 × MTT	[%]	–	43	46	47
Proportion of water older than 2 × MTT	[%]	–	22	25	27
SIGMA[c]	[‰]	–	0.086	0.137	0.247
EM[d]	[–]	–	0.81	0.74	0.32

[a] Weighted monthly mean values of Garmisch (1978–2009), corrected by elevation. All precipitation is assumed to infiltrate the aquifer and contribute to spring discharge; snow accumulation and snowmelt contribution is not taken into account

[b] Parameters calculated by using Eq. (1)

[c] Goodness of the fit, as described by Maloszewski and Zuber (2002)

[d] Efficiency of the model, as described by Maloszewski and Zuber (2002), EM=1 is ideal fit

 DOI 10.1007/s10040-014-1173-6

There is little drainage to the Bodenlaine Stream in the NE, as demonstrated by the results of injection in 1998. In this direction, drainage follows the dip of the fold axis; however, the stream is located at an elevation of 1,100–1,300 m asl. As a result, hydraulic gradients are lower in this direction, resulting in minor drainage to the Bodenlaine Stream. Additionally, springs are related to the upper stratigraphic unit. Positive detection of dye in the stream provides evidence for cross-formational flow. Flow must occur along strata boundaries, fractures and fault zones in order to cross the stratigraphic units (Fig. 9). Linear flow paths are conceivable. According to the local and regional flow pattern in mountainous areas studied by Tóth (1963, 1999), tracer may also enter deep flow paths and follow deep drainage structures to the receiving waters.

The presence of further flow paths is also indicated by moderate recoveries of about 20 % during each tracer test. The injected tracer uranine is an ideal tracer with conservative properties. Because tracer tests have demonstrated that karst drainage is related to fractures and fault zones, flow paths may occur along steep tectonic structures contributing to deep drainage and regional flow systems.

Results of the tracer test in 2011 constrain the relative thickness of the unsaturated zone. The tracer was injected close to the anticline structure in a central area of the mountains. As no tracer was detected in the southern valley, drainage in that direction is unlikely (Fig. 6). The saturated zone must be situated at great depth to prevent flow over the anticline structure to the south (Fig. 8). The thickness of the unsaturated zone is—in this part of the mountains—approximately as thick as the karst aquifer. Thus, the anticline acts as a water divide.

The quick breakthrough of the tracer combined with a long tail indicates that there is a large distribution of transit times dominating the drainage in the karst system. The fast-flow component is related to the karst drainage network consisting of conduits and open fissures; corresponding mean transit times are between 2 and 13 days (Fig. 13; Table 4). Turbulent flow in the core of conduits results in fast transport of water and solutes. The skewness of the BTCs is attributable to lower flow velocities, which occur due to laminar flow at margins of flow channels, flow through well-drained fractures and fissures, and fluid exchange with immobile fluid regions, e.g. dead-end passages. The fast-flow component is likely to affect spring water quality after precipitation events, as contaminants, e.g. fecal bacteria, are transported to the spring within a short period of time; thus, storage effects are low.

An intermediate- to slow-flow component has been delineated by tracer concentrations more than 1 year after the injection in 2011, indicating storage characteristics of the karst system. Percolation through the thick unsaturated zone, which consists of dipping strata, favors flow along strata boundaries and storage in poorly drained fissures, voids and joints (Fig. 13). In addition, pressure in water-filled fissures leads to conduit-matrix exchange. Owing to gradient inversion and matrix diffusion, water can be stored in the fissured rock matrix. With decreasing pressure in the drainage network, water is released out of the karst system slowly and, thus, contributes to base flow at springs.

An intermediate-flow regime is confirmed by stable isotope results that demonstrate long transit times in the karst system. Although there are uncertainties for the input and output signals, annual oscillation pattern of the isotopic signal at the springs is clearly visible. The signal is considerably dampened and shows a phase shift. The distinct output-signal at the springs indicates a dominant component of flow with a transit time of less than 1 year. The exponential model enables an estimation of the transit times, indicating that a significant proportion of the spring water has an approximate mean transit time between 2.9 and 4.9 months. Despite the uncertainties, a major flow component with transit times of a few months is in accordance with field observations of spring discharge characteristics. The proportion of the intermediate-flow component of spring discharge is roughly 50 %. This indicates that a large amount of new infiltrated water is released out of the karst system after a few months. Intermediate transit times are interpreted as a result of the mainly diffuse infiltration and drainage along numerous well-drained fissures and fractures of the karst system (Fig. 13; Table 4).

The results of the stable isotope modeling indicate that there is also a slow-flow component of the spring water that is older than the fresh infiltrated water and is probably older than a few years (Table 3). The presence of transit times of a few years is, furthermore, very likely (Maloszewski et al. 1983, 1992, 2002) and is in accordance with the conceptual model and triple porosity. The low-flow component with mean transit times in the range of years reflects diffuse infiltration in the poorly drained fissures and rock matrix of the aquifer. This flow component is particularly important with regard to long-term runoff characteristics of the alpine karst springs and impacts of climate change. High storage capability of the karstic Wetterstein limestone corresponds with observations of Rappl et al. (2010) and Maloszewski et al. (2002).

The average value for dispersion, determined by artificial tracer tests, is 126 m^2/h for the first peak and 539 m^2/h for the second one in 1998 (Table 2). In 2011, corresponding values are 4,011 and 3,334 m^2/h respectively. Dispersion is significantly higher in 2011 than in 1998 owing to higher flow velocities and slightly longer flow distances (300 m on average) in 2011. High flow velocities in the main flow channel are associated with large Peclet numbers ($Pe=vx/D_L$) between 17 and 73 (1st peak) and indicate high advective and turbulent flow in the core of the flow path; however, lower Peclet numbers between 8 and 21 arise with lower flow velocities and can be related to well-drained fissures and fractures along the flow path (2nd peak). To clarify dispersive flow, dispersivity ($\alpha=D_L/v$) is taken into account showing the same increase.

 DOI 10.1007/s10040-014-1173-6

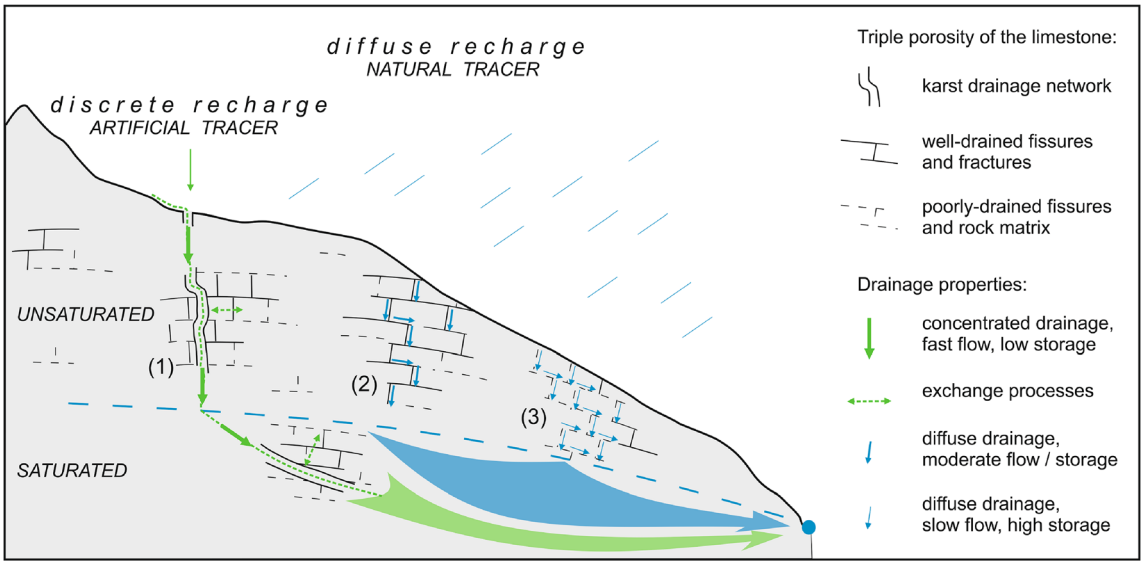

Fig. 13 Conceptual model of drainage in the investigated alpine karst system, showing triple porosity. *Numbers in parentheses* refer to Table 4

For the year 2011, mean transit times of uranine were used to calculation water volumes of the karst drainage network. Karst water volumes of about 100,000 m^3 were determined for the conduit network, whereas individual values range between 1,300 m^3 (S-2), 20,000 m^3 (S-4) and 74,000 m^3 (S-1; Fig. 13; Table 4). By using mean transit times of the natural tracer, it can be estimated that water volumes of well-drained fissures are significantly higher. Values lie between 90,000 m^3 (S-2) and 500,000 m^3 (S-4), excluding estimates for the waterfall and spring S-1, where isotopes could not be measured. These estimated water volumes are applicable for water in conduits and well-drained fissures in the Wetterstein Mountains. Most water is likely to be stored in poorly drained fissures and rock matrix (Maloszewski et al. 2002; Worthington 2007).

Conclusions

A combination of artificial and natural tracer investigations was performed in order to resolve drainage structures and transit time distribution of a high-alpine karst system. Underground drainage is not primarily linked with topographic divides: there are well-developed drainage structures crossing topographic divides and deep alpine valleys. Observed direction of flow is to the north showing that drainage occurs mainly in the direction of greatest hydraulic gradient to the deep gorge. Therewith, flow is linked to geologic weak zones and occurs transversely to the dip of the main fold axis. Flow is controlled by geologic structures in proximity to the main anticline structure, which acts as a water divide. Cross-formational flow from the main karst aquifer through the overlying formations towards discharge zones has been observed in the northeastern valley and probably occurs along numerous fractures and fault zones.

There is a fast-flow component draining karst conduits and open fissures. Mean transit times vary within several days and highly depend on flow conditions. Flow velocities increase by a factor of 2–5 under high flow conditions, owing to high precipitation and snowmelt in early summer. Considering the thickness of the unsaturated zone, the fast drainage is evidence for the presence of well-developed karst structures in the Wetterstein limestone. The long tailing of the BTCs is a result of slightly lower flow velocities, dominating on the margins of the karst conduit and well-drained fissures. As expected, calculated water volumes in the karst network are relatively low.

An intermediate-flow component has been identified, occurring along well-drained fissures and fractures of the aquifer. Mean transit times of the natural tracer are in the range of a few months. The drainage system benefits from

Table 4 Summary of the results from artificial and natural tracers characterizing a limestone with triple porosity. Numbers *1*, *2* and *3* refer to porosity, as shown in Fig. 13

	1	2	3
Flow path	Karst drainage network (conduits and open fractures)	Well-drained fissures and fractures	Poorly drained fissures and
Recharge	Discrete	Diffuse	Diffuse
Flow velocities	Fast flow: 180–1,050 m/day	Intermediate flow: 15–25 m/day	Slow flow: < 1 m/day
Mean transit time of tracer	2–13 days	2.9–4.9 months	A few years
Tracer	Uranine	Stable isotopes (^{18}O)	Indirecty determined (^{18}O)
Water volume	1,000 / 34,000 m^3 (S-2 / S-4)	90,000 / 500,000 m^3 (S-2 / S-4)	Not determined

 DOI 10.1007/s10040-014-1173-6

diffuse infiltration. A significant amount of water is stored in these well-drained fissures and contributes a great proportion to the spring discharge.

A slow-flow component is attributable to flow and storage in poorly drained fissures and rock matrix of the karst system. Mean transit times of the natural tracer of a few years are assigned to that flow component. Furthermore, persistent tracer concentrations of artificial tracer prove water storage in poorly drained fissures. Observed dilution effects after rain events are evidence for conduit-matrix exchange owing to gradient inversion. Poorly drained fissures and rock matrix are assumed to be the dominant reservoir for water.

The wide range of transit-time distribution demonstrates vulnerability in terms of runoff characteristics and contamination on the one hand and a potential of buffering hydrologic variability on the other hand. Short transit times, between a few days and a few months, reflect low storage capacity, high variability of spring discharge and fast transport of potential pollutants to the spring. Long transit times in the range of years demonstrate high storage capability in poorly drained fissures and therewith allow attenuation of extreme hydrologic events and retention of contaminants.

Acknowledgements The authors thank Zhao Chen and several students for their support during the fieldwork and Christine Stumpp from the Helmholtz Zentrum München, Germany, for providing isotopic data from Mt. Zugspitze and helpful comments. We further thank Klaus Fröhlich, MaryLynn Musgrove and an anonymous reviewer for valuable review comments and discussions.

References

Bakalowicz M (2005) Karst groundwater: a challenge for new resources. Hydrogeol J 13(1):148–160. doi:10.1007/s10040-004-0402-9

Bates BC, Kundzewicz Z, Wu S, Palutikof J (2008) Climate change and water. IPCC technical paper VI. IPCC Secretariat, Geneva, 210 pp

Bögel H (1960) Der geologische Bau des Wettersteingebirges und seiner Umgebung [The geological structure of the Wettersteingebirges and its surroundings]. Jb D Ö A V München 80:20–27

Dewalle DR, Edwards PJ, Swistock BR, Aravena R, Drimmie RJ (1997) Seasonal isotope hydrology of three Appalachian forest catchments. Hydrol Process 15:1895–1906. doi:10.1002/(SICI)1099-1085(199712)11:15<1895::AID-HYP538>3.3.CO;2-R

Einsiedl F (2005) Flow system dynamics and water storage of a fissured-porous karst aquifer characterized by artificial and environmental tracers. J Hydrol 312:312–321. doi:10.1016/j.jhydrol.2005.03.031

Field MS, Nash SG (1997) Risk assessment methodology for karst aquifers: 1. estimating karst conduit-flow parameters. Environ Monit Assess 47:1–21. doi:10.1023/A:1005753919403

Field MS, Pinsky PF (2000) A two-region nonequilibrium model for solute transport in solution conduits in karstic aquifers. J Contamn Hydrol 44:329–351. doi:10.1016/S0169-7722(00)00099-1

Field MS, Leij FJ (2012) Solute transport in solution conduits exhibiting multi-peaked breakthrough curves. J Hydrol 440:26–35. doi:10.1016/j.jhydrol.2012.03.018

Finger D, Heinrich G, Gobiet A, Bauder A (2012) Projections of future water resources and their uncertainty in a glacierized catchment in the Swiss Alps and the subsequent effects on hydropower production during the 21st century. Water Resour Res 48, W02521. doi:10.1029/2011WR010733

Frisch W, Kuhlemann J, Dunkl I (2008) Die geomorphologische Entwicklung der Ostalpen [The geomorphological evolution of the Eastern Alps]. Mitt österreich Geogr Ges 150:123–162

Geyer T, Birk S, Licha T, Liedl R, Sauter M (2007) Multitracer test approach to characterize reactive transport in karst aquifers. Ground Water 45(1):36–45. doi:10.1111/j.1745-6584.2006.00261.x

Goldscheider N (2005) Fold structure and underground drainage pattern in the alpine karst system Hochifen-Gottesacker. Eclogae Geol Helv 98(1):1–17. doi:10.1007/s00015-005-1143-z

Goldscheider N (2011) Alpine Hydrogeologie [Alpine hydrogeology]. Grundwasser 16:1–1. doi:10.1007/s00767-010-0157-2

Goldscheider N, Neukum C (2010) Fold and fault control on the drainage pattern of a double-karst-aquifer system, Winterstaude, Austrian Alps. Acta Carsolog 39(2):173–186

Goldscheider N, Brosemer M, Umlauf N, Hötzl H (1999) Karstentwässerung im Gebiet der Alpspitze (Wettersteingebirge, bayerische Kalkhochalpen) [Karst drainage in the area of alpine peaks (Wettersteingebirge, bayerische kalkhochalpen)]. Laich Höhlenfreund 34(2):47–68

Göppert N, Goldscheider N (2008) Solute and colloid transport in karst conduits under low- and high-flow conditions. Ground Water 46(1):61–68. doi:10.1111/j.1745-6584.2007.00373.x

Gremaud V, Goldscheider N, Savoy L, Favre G, Masson H (2009) Geological structure, recharge processes and underground drainage of a glacierised karst aquifer system, Tsanfleuron-Sanetsch, Swiss Alps. Hydrogeol J 17(8):1833–1848. doi:10.1007/s10040-009-0485-4

Grüger E, Jerz H (2010) Untersuchung einer Doline auf dem Zugspitzplatt: ein palynologischer Beitrag zur holozänen Gletschergeschichte im Wettersteingebirge [Investigation of a doline on the Zugspitzplatt: a palynological contribution to the Holocene glacial history of the Wettersteingebirge]. Quat Sci J 59:66–75. doi:10.3285/eg.59.1-2.06

Hagg W, Mayer C, Mayr E, Heilig A (2012) Climate and glacier fluctuations in the Bavarian Alps in the past 120 years. Erdkunde 66(2):121–142. doi:10.3112/erdkunde.2012.02.03

Käss W (2004) Geohydrologische Markierungstechnik [Textbook of geohydrological marking and tracing techniques]. Borntraeger, Stuttgart, 557 pp

Kraller G, Warscher M, Kunstmann H, Vogl S, Marke T, Strasser U (2012) Water balance estimation in high alpine terrain by combining distributed modeling and a neural network approach (Berchtesgaden Alps, Germany). Hydrol Earth Syst Sci 16:1969–1990. doi:10.5194/hess-16-1969-2012

Kübeck C, Maloszewski PJ, Benischke R (2013) Determination of the conduit structure in a karst aquifer based on tracer data: Lurbach system, Austria. Hydrol Process 27(2):225–235. doi:10.1002/hyp.9221

Küfmann C (2003) Soil types and eolian dust in high-mountainous karst of the northern calcareous alps (Zugspitzplatt, Wetterstein Mountains, Germany). Catena 53(3):211–227. doi:10.1016/S0341-8162(03)00075-4

Maloszewski P, Zuber A (1982) Determining the turnover time of groundwater systems with the aid of environmental tracers: 1. models and their applicability. J Hydrol 57(3–4):207–231. doi:10.1016/0022-1694(82)90147-0

Maloszewski P, Zuber A (2002) Manual on lumped-parameter models used for the interpretation of environmental tracer data in groundwaters. In: Yurtsever Y (ed) Use of isotopes for analyses of flow and transport dynamics in groundwater systems. IAEA, Vienna, pp 1–50

Maloszewski P, Rauert W, Stichler W, Herrmann A (1983) Application of flow models in an alpine catchment area using tritium and deuterium data. J Hydrol 66:310–330. doi:10.1016/0022-1694(83)90193-2

Maloszewski P, Rauert W, Trimborn P, Herrmann A, Rau R (1992) Isotope hydrological study of mean transit times in an alpine basin (Wimbachtal, Germany). J Hydrol 140:343–360. doi:10.1016/0022-1694(92)90247-S

Maloszewski P, Stichler W, Zuber A, Rank D (2002) Identifying the flow systems in a karstic-fissured-porous aquifer, the Schneealpe, Austria, by modelling of environmental ^{18}O and ^{3}H isotopes. J Hydrol 256(1–2):48–59. doi:10.1016/S0022-1694(01)00526-1

Marke T, Strasser U, Kraller G, Warscher M, Kunstmann H, Franz H, Vogel M (2013) The Berchtesgaden National Park (Bavaria, Germany): a platform for interdisciplinary catchment research. Environ Earth Sci 69(2):679–694. doi:10.1007/s12665-013-2317-z

Massei N, Wang HQ, Field MS, Dupont JP, Bakalowicz M, Rodet J (2006) Interpreting tracer breakthrough tailing in a conduit-dominated karstic aquifer. Hydrogeol J 14(6):849–858. doi:10.1111/j.1745-6584.2006.00291.x

Miller H (1961) Der Bau des westlichen Wettersteingebirges. Dt geol Ges Hannover 113:409–426

Mudarra M, Andreo B (2011) Relative importance of the saturated and the unsaturated zones in the hydrogeological functioning of karst aquifers: the case of Alta Cadena (southern Spain). J Hydrol 397(3–4):263–280. doi:10.1016/j.jhydrol.2010.12.005

Mudarra M, Andreo B, Marín AI, Vadillo I, Barberá JA (2014) Combined use of natural and artificial tracers to determine the hydrogeological functioning of a karst aquifer: the Villanueva del Rosario system (Andalusia, southern Spain). Hydrogeol J. doi:10.1007/s10040-014-1117-1

Müller MH, Weingartner R, Alewell C (2013) Importance of vegetation, topography and flow paths for water transit times of base flow in alpine headwater catchments. Hydrol Earth Syst Sci 17(4):1661–1679. doi:10.5194/hess-17-1661-2013

Ozyurt NN, Bayari CS (2008) Temporal variation of chemical and isotopic signals in major discharges of an alpine karst aquifer in Turkey: implications with respect to response of karst aquifers to recharge. Hydrogeol J 16(2):297–309. doi:10.1007/s10040-007-0217-6

Perrin J, Pochon A, Jeannin P-Y, Zwahlen F (2004) Vulnerability assessment in karstic areas: validation by field experiments. Environ Geol 46:237–245. doi:10.1007/s00254-004-0986-3

Plan L, Decker K, Faber R, Wagreich M, Grasemann B (2009) Karst morphology and groundwater vulnerability of high alpine karst plateaus. Environ Geol 58(2):285–297. doi:10.1007/s00254-008-1605-5

Pronk M, Goldscheider N, Zopfi J (2007) Particle-size distribution as indicator for fecal bacteria contamination of drinking water from karst springs. Environ Sci Technol 41(24):8400–8405. doi:10.1021/es071976f

Pronk M, Goldscheider N, Zopfi J, Zwahlen F (2009) Percolation and particle transport in the unsaturated zone of a karst aquifer. Ground Water 47(3):361–369. doi:10.1111/j.1745-6584.2008.00509.x

Schürch M, Kozel R, Schotterer U, Tripet J-P (2003) Observations of isotopes in the water cycle: the Swiss National Network (NISOT). Environ Geol 45:1–11. doi:10.1007/s00254-003-0843-9

Rappl A, Wetzel K-F, Büttner G, Scholz M (2010) Dye tracer investigations at the Partnach Spring (German Alps). HyWa 54(4):220–230

Rodgers P, Soulsby C, Waldron S (2005) Stable isotope tracers as diagnostic tools in upscaling flow path understanding and residence time estimates in a mountainous mesoscale catchment. Hydrol Process 19(11):2291–2307. doi:10.1002/hyp.5677

Simsek C, Elci A, Gunduz O, Erdogan B (2008) Hydrogeological and hydrogeochemical characterization of a karstic mountain region. Environ Geol 54(2):291–308. doi:10.1007/s00254-007-0817-4

Toride N, Leij F, van Genuchten M (1999) The CXTFIT code (version 2.1) for estimating transport parameters from laboratory or field tracer experiments. Research report no. 137, US Salinity Laboratory, Agricultural Research Service, USDA, Riverside, CA, 119 pp

Tóth J (1963) A theoretical analysis of groundwater flow in small drainage basins. J Geophys Res 68(16):4795–4812. doi:10.1029/JZ068i008p02354

Tóth J (1999) Groundwater as a geologic agent: an overview of the causes, processes, and manifestations. Hydrogeol J 7:1–14. doi:10.1007/s100400050176

Trček B, Zojer H (2009) Recharge of springs. In: Kresic N, Z Stevanovic (eds) Groundwater hydrology of springs. Elsevier, Amsterdam, pp 87–127

Vidal H (1953) Neue Ergebnisse zur Stratigraphie und Tektonik des nordwestlichen Wettersteingebirges und seines Vorlandes [New stratigraphic and tectonic findings in the northwestern Wetterstein Mountains and the foreland]. Geol Bavarica München 17:56–88

Viviroli D, Weingartner R (2004) The hydrological significance of mountains: from regional to global scale. Hydrol Earth Syst Sci 8(6):1016–1029. doi:10.5194/hess-8-1017-2004

Wetzel K (2004) On the hydrogeology of the Partnach area in the Wetterstein Mountains (Bavarian Alps). Erdkunde 58:172–186

Worthington S (2007) Groundwater residence times in unconfined carbonate aquifers. J Cave Karst Stud 69(1):94–102